JOURNAL OF ENZYME INHIBITION AND MEDICINAL CHEMISTRY
2026, VOL. 41, NO. 1, 2664708
https://doi.org/10.1080/14756366.2026.2664708

Taylor & Francis
by informa

RESEARCH ARTICLE

OPEN ACCESS Check for updates

Targeting ALDH7A1 with covalent inhibitors reveals new chemical space for prostate cancer therapy

Raffaella Gallo[a#], Antonio Scarano[b#], Eleonora Gianquinto[c], Gaia Franzini[d], Giulia Antonini[e], Serena Montalbano[e], Camillo Palmieri[a], Paola Conti[e], Francesca Spyrakis[c], Chiara Borsari[e] and Stefano Bruno[b,d]

[a]Department of Experimental and Clinical Medicine, "Magna Græcia" University of Catanzaro, Catanzaro, Italy; [b]Department of Food and Drug, University of Parma, Parma, Italy; [c]Department of Drug Science and Technology, University of Turin, Turin, Italy; [d]Biopharmanet-TEC, University of Parma, Parma, Italy; [e]Department of Pharmaceutical Sciences, University of Milan, Milan, Italy

ABSTRACT

Prostate cancer (PCa) remains a major global health burden. Although androgen deprivation and receptor-targeted therapies initially benefit patients, resistance often leads to metastatic castration-resistant prostate cancer, with limited treatment options. Aldehyde dehydrogenase 7A1 (ALDH7A1) is an emerging oncogenic driver of PCa, but selective inhibitors are lacking. Here, we report irreversible ALDH7A1 inhibitors targeting the catalytic Cys330, identified from a library of 3-bromo-4,5-dihydroisoxazole derivatives. These compounds show minimal inhibition of ALDH4A1 and GAPDH, supporting selectivity for ALDH7A1. Compounds **3b** and **4b** reduced DU145 cell viability (low μM IC_{50}), impaired migration, and altered the cell cycle. No significant effects were observed in LNCaP cells (low ALDH7A1 expression) or Hs27 fibroblasts. Treatment of DU145 cells resulted in the inhibition of intracellular ALDH activity and accumulation of malondialdehyde, consistent with increased oxidative stress. These findings validate ALDH7A1 as a druggable target and introduce a new chemical space for selective covalent ALDH inhibitors in oncology.

GRAPHICAL ABSTRACT

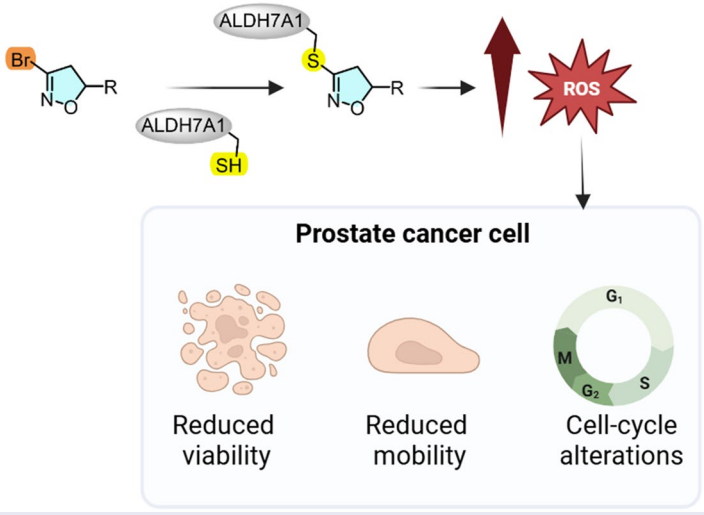

ARTICLE HISTORY
Received 28 January 2026
Revised 2 April 2026
Accepted 20 April 2026

KEYWORDS
ALDH7A1 selective inhibition; covalent enzyme inhibitors; 3-halo-4,5-dihydroisoxazoles; catalytic cysteine targeting; aldehyde dehydrogenase isoforms

CONTACT Stefano Bruno stefano.bruno@unipr.it Dept. of Food and Drug, Parco Area delle Scienze 23\a, Parma, Italy; Chiara Borsari chiara.borsari@unimi.it Dept. of Pharmaceutical Sciences, University of Milan, Via Mangiagalli 25, 20133 Milan, Italy
[#]These authors contributed equally to this work.

Supplemental data for this article can be accessed online at https://doi.org/10.1080/14756366.2026.2664708.

Introduction

Prostate cancer (PCa) is the second most common type of cancer and the fifth leading cause of cancer-related mortality in men, with an estimated 1.5 million new cases and 397,000 deaths worldwide in 2022 alone[1]. PCa typically arises as a localised disease but may progress to a locally advanced stage involving adjacent tissues such as the bladder, seminal vesicles, or the rectum. In more aggressive cases, PCa can metastasise through the lymphatic system to distant organs, including bones, lungs, and liver. While localised or locally advanced PCa is often curable, the metastatic disease remains largely fatal[2,3]. The Androgen Receptor (AR) signalling axis plays a central role in PCa initiation, progression, and metastatic progression. AR is a ligand-activated transcription factor that regulates the expression of genes involved in cell proliferation and survival upon binding of androgens[4]. Consistently, standard therapies involve androgen deprivation therapy (ADT) and AR inhibitors, often in combination with chemotherapy or radiotherapy[5,6]. Although AR-targeted therapies yield initial clinical benefits, many patients eventually develop resistance, culminating in the emergence of metastatic castration-resistant PCa (mCRPC), which is associated with significantly reduced survival. Growing evidence indicates that hormone deprivation is frequently associated with oxidative stress, marked by elevated levels of reactive oxygen species (ROS) and enhanced redox signalling. This oxidative environment contributes to the modulation of autophagy, inflammation, and cellular stress responses, ultimately promoting the survival and proliferation of PCa cells with metastatic potential[7,8]. The intricate interplay between androgen signalling and redox homeostasis underscores the urgent need for more effective therapeutic strategies and the identification of novel drug targets to overcome treatment resistance and improve patient outcomes.

Aldehyde dehydrogenases (ALDHs) are a family of enzymes involved in detoxification of ROS, specifically aldehydes, within the cell. In humans, 19 ALDH isoforms have been identified, each distinguished by different substrate preference and involvement in human pathologies[9]. In addition to serving as biomarkers of cancer stem-like cells, ALDHs also participate directly in signal transduction pathways that regulate key biological activities of PCa cells. For instance, ALDH1A1 and ALDH1A3 have been shown to regulate retinoic acid, WNT/β-catenin, and PI3K/AKT signalling pathways, while ALDH3A1 is frequently upregulated in prostate cancer stem-like cells and metastatic lesions and has been associated with prostate tumorigenesis[10–15].

ALDH7A1 (ALDH7A1, Uniprot P49419, EC 1.2.1.31) catalyses the conversion of 4-hydroxynonenal (4-HNE), a byproduct of lipid peroxidation, into less toxic metabolites, thereby playing a crucial role in cellular protection from oxidative damage[16,17]. Consistently, ALDH7A1 has been implicated in PCa progression. Large-scale proteomic profiling of human prostate cancer specimens has identified ALDH7A1 as one of the most abundantly expressed ALDH enzymes in primary tumours[18]. Transcriptomic data demonstrated robust ALDH7A1 mRNA expression in PCa tissues, with significantly higher levels observed in cancerous lesions compared with benign prostatic hyperplasia (BPH) or histologically normal adjacent prostate tissue[19]. Functionally, it has been shown that ALDH7A1 promoted stemness and migratory capacity in PCa cells, and its targeted deletion impaired clonogenicity, and significantly reduced tumour growth, supporting a potential oncogenic role[20,21]. Particularly, knockdown of ALDH7A1 reduced experimentally induced PCa bone metastasis[21]. Consistent with the hypothesis that ALDH7A1 inhibition may enhance oxidative stress and limit tumour cell growth, salinomycin-induced oxidative stress markedly impaired PCa cell proliferation[22].

To date, only a limited number of reversible and irreversible inhibitors of ALDH7A1 have been identified, and most of them are considered pan-ALDH inhibitors. For instance, diethylaminobenzaldehyde (DEAB) was identified as an inhibitor of ALDH7A1 and forms an acyl-enzyme covalent adduct with the catalytic Cys330, as determined by X-ray crystallography[23]. However, DEAB also inhibited other ALDH isoforms[24,25], and its small molecular size offers limited potential for structural optimisation towards isoform-selectivity. Although targeting ALDHs in PCa cells holds therapeutic potential, challenges remain due to isoform redundancy, toxicity of non-selective inhibitors, and incomplete understanding of ALDH-related signalling networks[26,27].

Aiming to identify selective ALDH7A1 inhibitors, we chose acivicin (ACV) as a starting point. ACV is an analogue of glutamate/glutamine featuring a 3-chloro-4,5-dihydroisoxazole scaffold. This natural antiproliferative compound, isolated from *Streptomyces* species, was previously reported as an *in vivo* inhibitor of aldehyde dehydrogenase 4A1 (ALDH4A1), a paralog of ALDH7A1[27]. Although ACV exhibited anticancer

activity *in vitro*, its clinical development was hampered by significant toxicity observed in Phase I trials[28]. Besides ALDH4A1, which has γ-glutamate semialdehyde as substrate, ACV inhibits other glutamine or glutamate-dependent enzymes, including glutamine synthase[29], CTP synthetase[30], GMP synthetase, asparagine synthetase, and γ-glutamyl transpeptidase[31,32]. These enzymes generally exhibit a catalytic dyad or triad which includes a cysteine residue. The nucleophilic attack of the cysteine thiol at C3 of the 4,5-dihydroisoxazole nucleus leads to the displacement of the chlorine atom and the covalent bond formation[33] (Figure 1). The study identifying ALDH4A1 as the primary *in vivo* target of ACV also reported 3-bromo-ACV (3-BA) derivatives as ALDH inhibitors with a mechanism of action similar to that of ACV[34] (Figure 1), thus supporting their evaluation as potential ALDH7A1 inhibitors.

We have previously shown that the substituents on the 3-bromo-4,5-dihydroisoxazole (BDHI) ring modulate its reactivity towards the reactive cysteines of glyceraldehyde 3-phosphate dehydrogenase (GAPDH) [35–39], suggesting the possibility to fine-tune the selectivity also towards ALDH isoforms. In this study, we selected a series of compounds from an in-house library of 3-BA analogs and investigated their activity against ALDH7A1 in comparison with ALDH4A1 and GAPDH. We evaluated their effects both *in vitro* and in PCa cell lines, aiming to pave the way for the development of novel selective ALDH7A1 inhibitors for the treatment of PCa.

Results and discussion

Expression and characterisation of the enzymes

To investigate human ALDH7A1 inhibition, the enzyme was recombinantly expressed and purified (Figure S1a). For comparison, human ALDH4A1 and human GAPDH were also produced. These enzymes were included in the screening assays since ACV and its analogs were originally reported to inhibit ALDH4A1[34], whereas GAPDH was identified as a target of BDHI derivatives, some of which markedly reduced tumour growth in mouse xenograft models without detectable toxicity in fibroblasts or *in vivo*[35–39].

Size-exclusion chromatography (SEC) of ALDH7A1 analysed at a 5 µM concentration yielded an apparent molecular weight of 121.4 kDa, consistent with its dimeric state (theoretical MW 112.9 kDa, Figure S1b). At higher concentrations (18 µM and 83 µM), higher apparent MWs of 148.8 kDa and 170.4 kDa were observed (Figure S1b), respectively, consistently with reports of a dimer-tetramer equilibrium with a dissociation constant of approximately 16 µM[40]. Therefore, the enzyme at the concentrations used in all our assays (0.5–1 µM) was confirmed to be in the dimeric form.

For ALDH7A1, we optimised an enzyme assay based on acetaldehyde (AcH) as substrate, resulting in a Michaelis constant (K_m) of 2.1 ± 0.5 mM and a turnover number (k_{cat}) of 0.15 s^{-1} (Figure S1c). All inhibition assays were performed at a 10 mM AcH concentration, corresponding to near-saturating conditions and approximating V_{max}. For ALDH4A1, we established an enzyme assay employing its physiologically relevant substrate Δ^1-pyrroline-5-carboxylate (P5C), while GAPDH enzyme assays were performed using glyceraldehyde 3-phosphate (G3P), NAD^+ and arsenate as substrates, following previously described protocols[35].

In vitro *activity of ACV and 3-BA towards the recombinant enzymes*

ALDH7A1, ALDH4A1 and GAPDH were incubated with ACV or 3-BA (Figure 2a) at 20 µM for 24 h at 37 °C, under conditions designed to mimic those employed in subsequent cell-based experiments. Under these

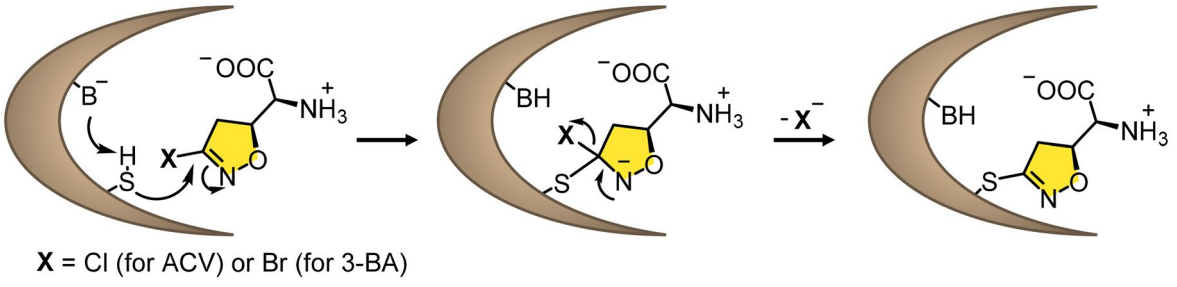

Figure 1. Mechanism of inhibition by 3-BA through direct modification of the active site nucleophile (cysteine). B: base.

conditions, ALDH7A1 activity was unaffected by ACV or 3-BA (Figure 2b), whereas ALDH4A1 showed modest inhibition (≈20% with ACV and ≈30% with 3-BA; Figure 2c), consistently with previous reports identifying ALDH4A1 as the primary *in vivo* target of ACV[34]. We speculated that the different behaviour towards ALDH7A1 and ALDH4A1 may arise from the marked difference in hydrophilicity and polarity of ACV and 3-BA (negative cLogD; Table 1). Under the same conditions, GAPDH was not inhibited (Figure 2d). Overall, these results ruled out ACV and 3-BA as inhibitors of ALDH7A1 and highlighted the need to identify novel BDHI derivatives capable of effectively reducing ALDH activity in PCa, while maintaining negligible activity towards GAPDH, a ubiquitous enzyme whose inhibition might be associated with side effects.

Inspection of the ALDH7A1 structure and identification of the inhibitor library

To identify a novel chemical space for 3-BA analogs as inhibitors of ALDH7A1, we explored the 3D structure of the enzyme (PDB 4ZUK), which revealed an active site featuring a solvent-accessible pocket extending from the catalytic Cys330 to the protein surface. A key structural element is a ~15 Å-long hydrophobic channel lining one end of the pocket, which contributes to substrate positioning and selectivity[41]. This structural feature may favour the binding of hydrophobic compounds to ALDH7A1 compared with ALDH4A1, as also suggested by the relatively hydrophilic nature of the physiologically relevant ALDH4A1 substrate, L-glutamate-γ-semialdehyde, in contrast to the more hydrophobic substrates of ALDH7A1, which include α-aminoadipate (α-AA), nonanal, trans-2-nonenal, hexanal, octanal, benzaldehyde, and propanal[42]. We could not confirm betaine aldehyde as a substrate[42] at concentrations up to

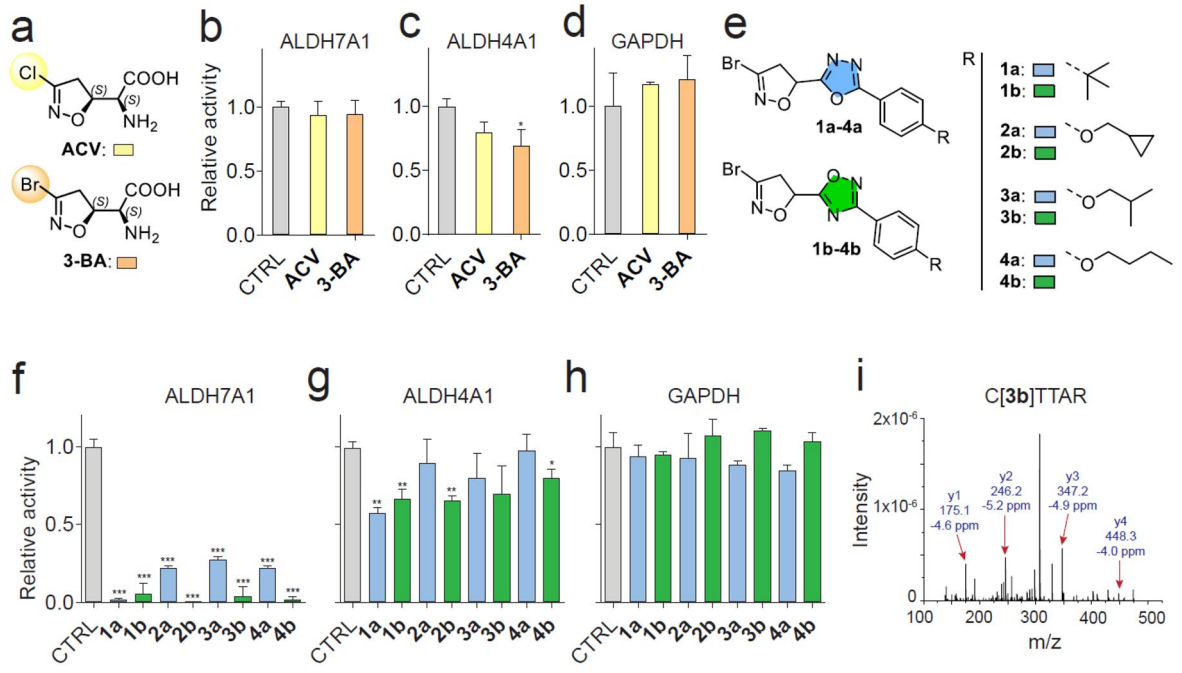

Figure 2. (a). Chemical structures of ACV and 3-BA. (b–d) Inhibition of human ALDH7A1 (b), ALDH4A1 (c), and GAPDH (d) by ACV and 3-BA. Enzymes were incubated at 2.5 µM with 20 µM of each compound at 37 °C for 24 h, and residual activity was measured under standard assay conditions and normalised to control incubations containing equivalent concentrations of DMSO. Bars represent mean values; error bars indicate standard deviation from at least two independent experiments, each in technical duplicate. Statistical significance was evaluated using Student's T-test. Asterisks indicate statistical significance levels compared with the control: $p \leq 0.05$ (*), $p \leq 0.01$ (**), $p \leq 0.001$ (***), and $p \leq 0.0001$ (****). (e) Structures of all compounds tested in this study. (f–h) Effect of selected compounds on human ALDH7A1 (f), ALDH4A1 (g), and GAPDH (h) after incubation at 2.5 µM enzyme concentration with 20 µM compounds at 37 °C for 24 h; residual activity is expressed as a fraction of the untreated control containing equivalent concentrations of DMSO, with bars representing mean values and error bars indicating standard deviation from at least two independent experiments, each performed in technical duplicate. Statistical significance was evaluated using Student's T-test. (i). MS/MS spectrum of the modified CTTAR peptide obtained by HCD fragmentation; observed *y* ions confirm the peptide sequence and localise the covalent modification to Cys330 of ALDH7A1, consistent with the formation of an irreversible adduct. Fragment ion annotation and match scores were obtained using the software Skyline.

Table 1. Chemical structure of ACV, 3-BA and selected molecules from our BDHI in-house library.

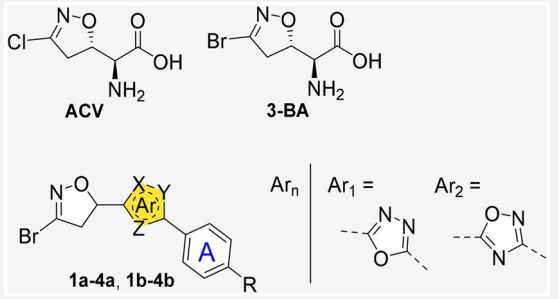

Comp.	Ar_n	R	clogD[a]
ACV	–	–	−2.96
3-BA	–	–	−2.67
1a	Ar_1		3.35
1b	Ar_2		4.84
2a	Ar_1	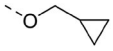	2.42
2b	Ar_2		3.81
3a	Ar_1	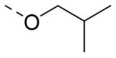	2.89
3b	Ar_2		4.28
4a	Ar_1	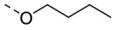	2.97
4b	Ar_2		4.31

[a]Marvin/JChem 20.9 was used to calculate logD (distribution coefficient, pH 7.4) values. ChemAxon (https://www.chemaxon.com).

10 mM (data not shown). Therefore, starting from our in-house library of BDHI-bearing molecules, we selected a panel of 1,3,4- and 1,2,4-oxadiazole matched pairs (Table 1, Figure 2e) which exhibit high lipophilicity (cLogD > 2, Table 1). Oxadiazoles are five-membered aromatic heterocycles existing in different regioisomeric forms, commonly found in drug-like compounds[43].

Investigation of the ALDH7A1 inhibitory activity of the compounds

Following incubation at a final concentration of 20 µM, all test compounds inhibited recombinant ALDH7A1 activity > 70% (Figure 2f). Among them, the 1,2,4-oxadiazole derivatives **2b-4b** inhibited > 92–98%, while their corresponding 1,3,4- isomers showed a lower inhibitory activity in the 70–90% range. The higher potency of the 1,2,4- regioisomers, which typically have a higher cLogP when compared to their 1,3,4-isomer counterparts, confirmed the importance of lipophilicity in binding to the ALDH7A1 isoform (see cLogP comparison in Table 1). For the tert-butyl substituted derivatives (**1a** and **1b**), both 1,2,4- and 1,3,4-isomers produced >90% inhibition. All compounds displayed significantly higher activity against ALDH7A1 compared to that of ACV and 3-BA against ALDH4A1 (Figure 2g). Therefore, we disclosed a novel chemical space for ALDH7A1 inhibitors.

Assessment of selectivity and investigation of off-target effects

Afterwards, we assessed the selectivity of the library for ALDH7A1 over GAPDH and ALDH4A1. None of the BDHI compounds targeting ALDH7A1 showed significant inhibition of GAPDH under the same assay conditions (Figure 2d). ALDH4A1 inhibition was minimal: only **1a** induced a statistically significant inhibition of ~30% (Figure 2g). Overall, these results indicate that structural modifications on the BDHI ring enhanced the selectivity of the compounds for ALDH7A1 in comparison with ALDH4A1, reversing the inhibition profile of ACV and 3-BA towards the two paralogs, while maintaining no activity towards GAPDH.

Confirmation of covalent Cys330 engagement

Since compound **3b** emerged as one of the most promising and selective inhibitors, it was pinpointed as a representative example for LC-MS/MS experiments aimed at confirming the inhibition

mechanism. Firstly, ALDH7A1 was incubated with **3b**. The protein was then carbamidomethylated on unreacted cysteines with iodoacetamide and trypsin digested. Tandem mass spectrometry data spectra were searched against the ALDH7A1 sequence using carbamidomethylation and **3b** binding (+285.11 Da, according to the mechanism reported in Figure 1) as cysteine variable modifications. Among the identified **3b**-modified sites, only two cysteine-containing peptides were detected: (i) CTTAR (residues 330–334), containing the catalytic Cys330; and (ii) GEVITTYCPANNEPIAR (residues 70–85), containing cysteine 77. Peptide CTTAR was exclusively identified in its **3b**-modified form, exhibiting high precursor intensity (~731 million) and a high overall score (94.4), consistent with a highly abundant and specific modification at Cys330 (Figure 2i and Figure S2). In contrast, peptide GEVITTYCPANNEPIAR appeared predominantly in its carbamidomethylated form, with the **3b** modification detected only in a minor fraction of spectra. This **3b**-modified form showed significantly lower intensity (~26.5 million), a reduced score (57.8), and greater variability in mass accuracy, suggesting a low-efficiency or less stable modification at Cys70. Thus, Cys330, the catalytic cysteine residue, emerged as the principal site of **3b** adduct formation in ALDH7A1 and the reaction mechanism of the BDHI towards cysteine residues was confirmed (Figure 1).

Computational studies to rationalise ALDH isoform selectivity, stereospecificity and potency of the compounds

To rationalise the observed selectivity for ALDH7A1 over ALDH4A1, we carried out docking studies aimed at determining plausible binding orientations, analysing key stabilising interactions in the post-covalent complex, and comparing the steric and electrostatic environments of the two enzymes. As a starting point, we examined the deposited X-ray structures of both isoforms in complex with their product α-AA or glutamate, respectively (PDB IDs: 4ZUL and 3V9K; Figure 3(a)-b)[41,44]. In this section, the residue numbering of PDBs will be retained and thus the catalytic Cys330 will correspond to Cys302 in the PDB structures used hereafter. Despite modest sequence identity, both isoforms display a conserved architecture of the catalytic site, including a catalytic cysteine, an oxyanion hole comprising the backbone amide of the catalytic cysteine and a conserved asparagine, a substrate-anchoring loop, and an aromatic triad (known as 'aromatic box') that sandwiches the aliphatic chain of the substrate[45,46]. Lastly, stereoselectivity towards the L-substrate is assisted by electrostatic interactions of Glu165 and Lys347 in ALDH4A1[46], corresponding to Glu121 and Arg301 in ALDH7A1. Despite these similarities, ALDH7A1 can accommodate the α-aminoadipate (α-AA) product, which is one methylene unit longer than the glutamate (Glu) product of ALDH4A1. The substitution of Ser513 in ALDH4A1 with Ala462 in ALDH7A1 has been proposed to underlie substrate specificity between the isoforms and the preference for more polar substrates in ALDH4A1[41].

We first aimed at computationally studying the structural basis of ACV and 3-BA selectivity towards ALDH4A1 rather than ALDH7A1 via covalent molecular docking (Figure 3c-d). As it is generally known that NAD^+ binds before aldehyde substrates in ALDH enzymes, we chose to explicitly model the NAD^+ cofactor in the catalytic site in our docking studies. As expected, self-docking of glutamic aldehyde in ALDH4A1 showed the tetrahedral intermediate establishing hydrogen bonds with the oxyanion hole formed by the backbone of residue Cys348 and the side chain of Asn211 (Figure 3c), while the rest of the interactions remained unaltered with respect to the crystal pose of Glu in PDB 3V9K (Figure 3b). The productive tetrahedral intermediate is assumed to have a stereocenter in the *R*- configuration to enable hydride transfer to NAD^+, consistent with the A-specificity reported for ALDH4A1[47]. As reported above, *in vitro* assays indicated a modest inhibition of ALDH4A1 by ACV (≈20%) and 3-BA (≈30%), while the compounds were practically ineffective against ALDH7A1. Docking studies of ACV and 3-BA in ALDH4A1 showed hydrogen bonds with residues Gly512 and Ser513, likely important in the stabilisation of ACV and 3-BA (Figure 3d). We hypothesise that, given the presence of Ala462 instead of Ser in the anchoring loop in ALDH7A1, small and highly polar compounds such as ACV and 3-BA cannot be stabilised and correctly oriented for covalent binding, hence explaining their lack of activity in ALDH7A1.

We further sought to investigate the binding mode of the library of synthesised compounds in ALDH7A1. Initially, we self-docked the α-AA substrate in ALDH7A1, and results show that in the

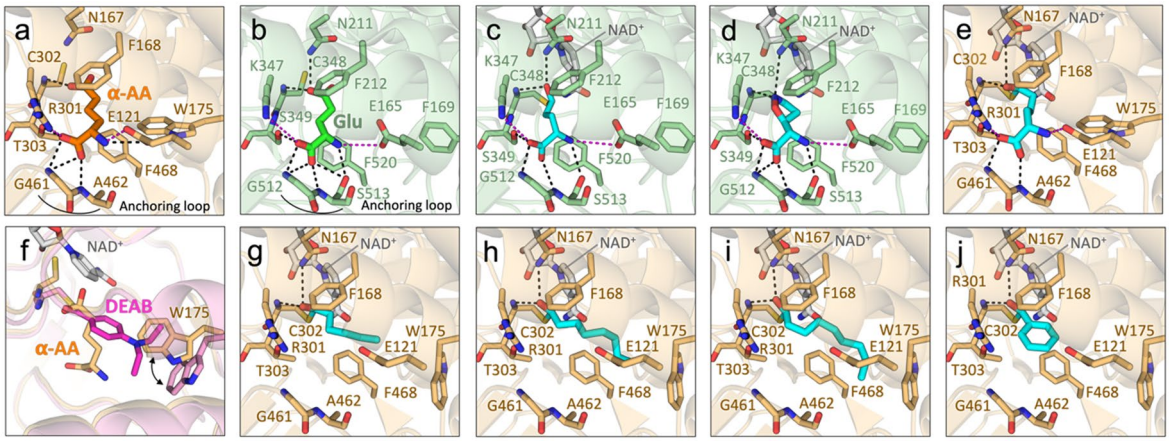

Figure 3. (a) Active site of ALDH7A1 in complex with the reaction product α-aminoadipate (α-AA, in sticks, orange) in PDB ID 4ZUL. Distances and angles compatible with hydrogen bonds are indicated with a black dashed line, while magenta dashed lines highlight ionic interactions. The anchoring loop (Gly461-Ala462) is indicated with a black line and labelled. (b) Active site of ALDH4A1 in complex with the reaction product glutamate (Glu, in sticks, green) in PDB ID 3V9K. The anchoring loop (Gly512-Ser513) is indicated with a black line and labelled. Covalent docking of ligands (in sticks, cyan): (c) glutamate-5-semialdehyde in ALDH4A1; (d) 3-BA in ALDH4A1; (e) α-aminoadipic semialdehyde in ALDH7A1; (f) hexanal in ALDH7A1; (g) octanal in ALDH7A1; (h) nonanal in ALDH7A1; (i) benzaldehyde in ALDH7A1. (j) Superposition of product-bound ALDH7A1 (PDB: 4ZUL, orange) and DEAB-bound ALDH7A1 (PDB: 4X0T, pink). Displacement of Trp175 is highlighted by a black arrow.

R-tetrahedral adduct derived by the nucleophile addition of Cys302 to the aldehyde carbonyl, the negatively charged oxygen is stabilised in the oxyanion hole formed by the backbone of Cys302 and Asn167 (Figure 3e). We next explored the binding modes of other ALDH7A1 substrates (hexanal, benzaldehyde, octanal and nonanal in Figure 3(g)-j). Their predicted poses differ from those of the native substrate, as these aldehydes lack the characteristic *L*-amino acid moiety required for the engagement of the anchoring loop. Instead, their orientation matches the binding mode of the ALDH7A1-diethylaminobenzaldehyde (DEAB) complex (PDB ID: 4X0T), in which DEAB occupies the aromatic box while the anchoring loop remains disengaged (Figure 3f). The ALDH7A1-DEAB complex X-ray structure further shows that hydrophobic and bulky ligands such as DEAB also displace Trp175 and expand the binding pocket through induced-fit effects.

Both *R*- and *S*-isomers of the synthesised compounds were covalently docked to ALDH7A1 via a nucleophilic substitution reaction on the BDHI ring by Cys302, and subsequent elimination of the halogen atom. However, we focused our analysis on *S*-isomers, which generally produced better occupancy of the oxyanion hole through nitrogen and oxygen H-bond acceptors on the BDHI warhead, consistent with the stereochemistry of ACV (see Figure S3). Short, rigid compounds **1a** and **1b** adopted a consistent binding mode in which the 1,3,4-oxadiazole mimics the α-AA carboxylate and interacts with Arg301 and the anchoring loop, while the 1,2,4-oxadiazole ring is enclosed between Phe168 and Phe468 through π–π stacking (Figure 4(a,e)). The 4-*tert*-butyl-phenyl substituent occupies the hydrophobic region of the pocket, with the phenyl ring stacking against Phe468 and the tert-butyl group contacting Ile464 and Trp175. In contrast, the addition of flexible lipophilic tails in compounds **2-4a** and **2-4b** produced a distinct pose (Figure 4b-d and f-h). Here, the oxadiazole and adjacent groups occupy a deeper hydrophobic region also exploited by DEAB in PDB 4X0T (Figure 3f). The BDHI ring still satisfies the oxyanion hole and the Phe168/Phe468 π–π stacking but is positioned farther from Arg301 and the anchoring loop. In this environment, the more lipophilic 1,2,4-oxadiazole regioisomer may be favoured over the more polar 1,3,4-oxadiazole. The flexible alkyl substituents (oxy-methyl-cyclopropyl-, isobutyl-, n-butyl-) fit into a narrow hydrophobic tunnel lined by Ile452, Ala462, Phe468 and Thr493, the same region occupied by the docking poses of long-chain alkyl aldehydes (see above). In ALDH4A1, the presence of Ser513 in place of Ala462 may alter both polarity and steric accessibility of this tunnel (Figure S4). This might restrict the entry of compounds **2-4a** and **2-4b**, rationalising their loss of activity in ALDH4A1 and the preference of ALDH7A1 for more lipophilic substrates.

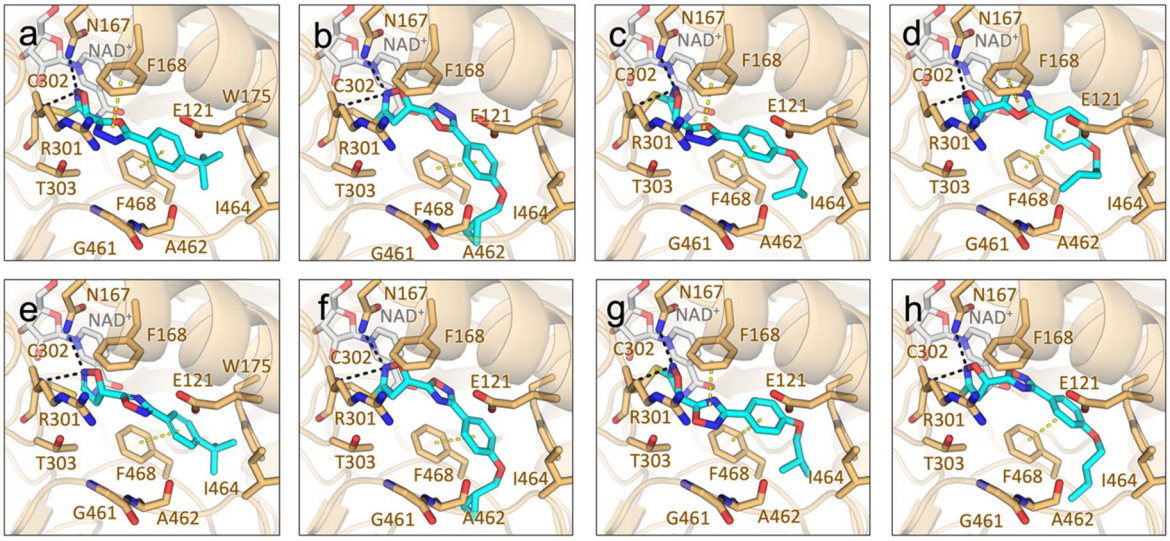

Figure 4. Covalent docking of the synthesised BDHI compounds in ALDH7A1. Protein is shown as cartoon and binding site residues are shown as sticks and labelled, NAD^+ cofactor is displayed as grey sticks, while docked ligands (*S*-isomers) are represented as cyan sticks. (a) **1a**; (b) **2a**; (c) **3a**; (d) **4a**; (e) **1b**; (f) **2b**; (g) **3b**; (h) **4b**.

Impact of the compounds on PCa cell line cell viability

To validate the *in vitro* and *in silico* findings in a cellular context, the DU145 PCa cell line was selected as a suitable model due to its high expression of ALDH7A1, as reported in the Human Protein Atlas (www.proteinatlas.org). A cell viability assay was performed to determine the half-maximal inhibitory concentration (IC_{50}) of each compound. DU145 cells were treated with increasing concentrations of the compounds (1–100 µM) for 24 h, and cell viability was assessed using a crystal violet assay. Compounds **1a**, **1b-4b** exhibited the lowest IC_{50} values, ranging from 13.5 to 20.9 µM. In contrast, the 1,3,4-oxadiazole derivative **2a-4a** displayed IC_{50} values > 50 µM, indicating minimal effect on DU145 cell growth (Figure S5a and Table 2). Interestingly, for the ether-substituted compounds, the replacement of the 1,2,4-oxadiazole core with the 1,3,4-oxadiazole ring led to a drop in the antiproliferative activity. These results are consistent with the *in vitro* data, which identified **1a**, **1b-4b** as the most potent ALDH7A1 inhibitors, whereas **2a-4a** were among the least effective in DU145 cells (Figure 2f). To assess whether the observed antiproliferative effects were dependent on cellular context, the activity of compounds **1a–4b** was also evaluated in the androgen receptor–positive prostate cancer cell line LNCaP. In contrast to DU145 cells, treatment with the compounds did not result in significant growth inhibition across the tested concentration range (Figure S5b). Notably, previous reports[48] and transcriptomic data from the Human Protein Atlas indicate that ALDH7A1 is expressed in DU145 cells but is absent or expressed at very low levels in LNCaP cells, consistent with the lack of sensitivity observed in this model (Figure S5c).

Based on both antiproliferative and recombinant protein activity assays, we selected the four most potent inhibitors (**1a**, **1b**, **3b** and **4b**) for further investigation.

Impact of compounds treatment on PCa cell line cell motility and cell cycle progression

To assess the ability of the selected compounds to reduce PCa cell motility, we performed a wound-healing assay in the presence of **1a**, **1b**, **3b** and **4b** or DMSO as a control, in DU145 cancer cells. Each of the tested compounds induced a decrease in cell migration and a less marked wound closure compared to the control (Figures 5a-b and S6a-b). Among the tested compounds, **3b** and **4b** exhibited the most pronounced inhibitory effects on wound closure, indicating reduced metastatic potential upon treatment (Figures 5a and b). Next, we evaluated the impact of the compounds on cell cycle progression. Cells were treated with **1a**, **1b**, **3b** and **4b** or DMSO for 24 h. Following fixation, cells were stained with propidium iodide (PI) and analysed by flow cytometry to determine the distribution across cell cycle phases (G1, S, and G2/M) as well as the proportion of cells exhibiting fragmented DNA (sub-G1 population).

Table 2. Antiproliferative activity towards DU145 cells.

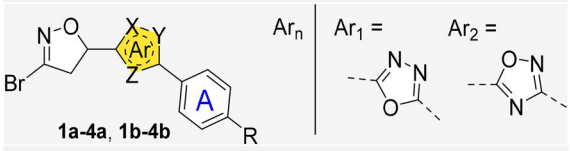

Comp.	Ar_n	R	IC_{50} ± SD (μM)
1a	Ar_1		19.7 ± 2.0
1b	Ar_2		14.6 ± 3.5
2a	Ar_1	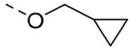	>50
2b	Ar_2		20.9 ± 7.6
3a	Ar_1	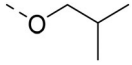	>50
3b	Ar_2		15.1 ± 1.6
4a	Ar_1	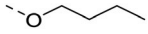	>50
4b	Ar_2		13.5 ± 5.1

Treatment with **1a** did not induce cell cycle abnormalities. In contrast, **1b** resulted in a modest reduction in the percentage of cells in the G1 phase accompanied by an increase in the G2/M population (Figure S6c). Both **3b** and **4b** treatment resulted in reduction of cells in the G2/M phase; notably, **4b** treatment also elicited a limited but significant increase in cells in the G1 phase (Figure 5c). Moreover, exposure to **3b** or **4b** led to a pronounced accumulation of cells in the sub-G1 fraction, indicative of an increase in the number of cells undergoing apoptosis or other forms of cell death (Figure 5c). The observed increase in sub-G1 population, most likely due to the accumulation of reactive oxygen species, is consistent with disruption of cellular redox homeostasis upon ALDH7A1 inhibition; however, long-term compensatory mechanisms may emerge, including upregulation of alternative ALDH isoforms or activation of cytoprotective pathways such as the NRF2-dependent antioxidant response[49]. Therefore, future investigations will be necessary to evaluate the *in vivo* therapeutic potential of these compounds.

Collectively, these results demonstrate an antiproliferative effect of the tested compounds in PCa cell lines, highlighting a more pronounced effect for **3b** and **4b.**

To evaluate the potential cytotoxicity of the compounds in non-tumoral cells, Hs27 fibroblasts were treated with increasing concentrations of compounds 3b and 4b under the same experimental conditions used for PCa cells. Both compounds exhibited minimal effects on cell viability across the tested concentration range, with IC_{50} values > 50 μM for **3b** and **4b** (Figure S7). These findings support a selective profile towards ALDH7A1-expressing cancer cells, such as DU145.

Inhibition of intracellular activity of ALDHs

To further confirm that the effects observed in DU145 cells were due to irreversible ALDH inhibition, we measured ALDH activity using AcH and NAD^+ as substrates in lysates from DU145 cells treated with **3b** or **4b** (20 μM, close to their IC_{50}) for 24 h, followed by extensive washing and lysis. The activity was normalised to the total protein content of each sample, as determined by Bradford assay. Compared to control cell samples treated with the DMSO only, treatment with **3b** resulted in a ~20% decrease in ALDH activity, while **4b** induced a more pronounced reduction of ~40% (Figure 5d).

Aldehyde-associated oxidative stress upon ALDH inhibition

Since ALDH7A1 was reported to detoxify reactive oxygen species (ROS)-derived lipophilic metabolites, we assessed the effect of **3b** or **4b** on the intracellular concentration of malondialdehyde (MDA), a lipid peroxidation product recognised as a key cancer marker linked to oxidative stress[50]. DU145 cells were treated with either **3b** or **4b** at a final concentration of 20 μM for 24 h, while control cells were treated with an equivalent concentration of DMSO. After cells were washed and lysed, MDA concentration was measured and normalised to the total protein concentration of each sample, as determined by Bradford assay. Cells pre-treated with **3b** or **4b** showed a 7-fold and 4-fold increase in MDA levels, respectively, compared to controls, indicating a marked rise in lipid peroxidation (Figure 5e). Similar results were

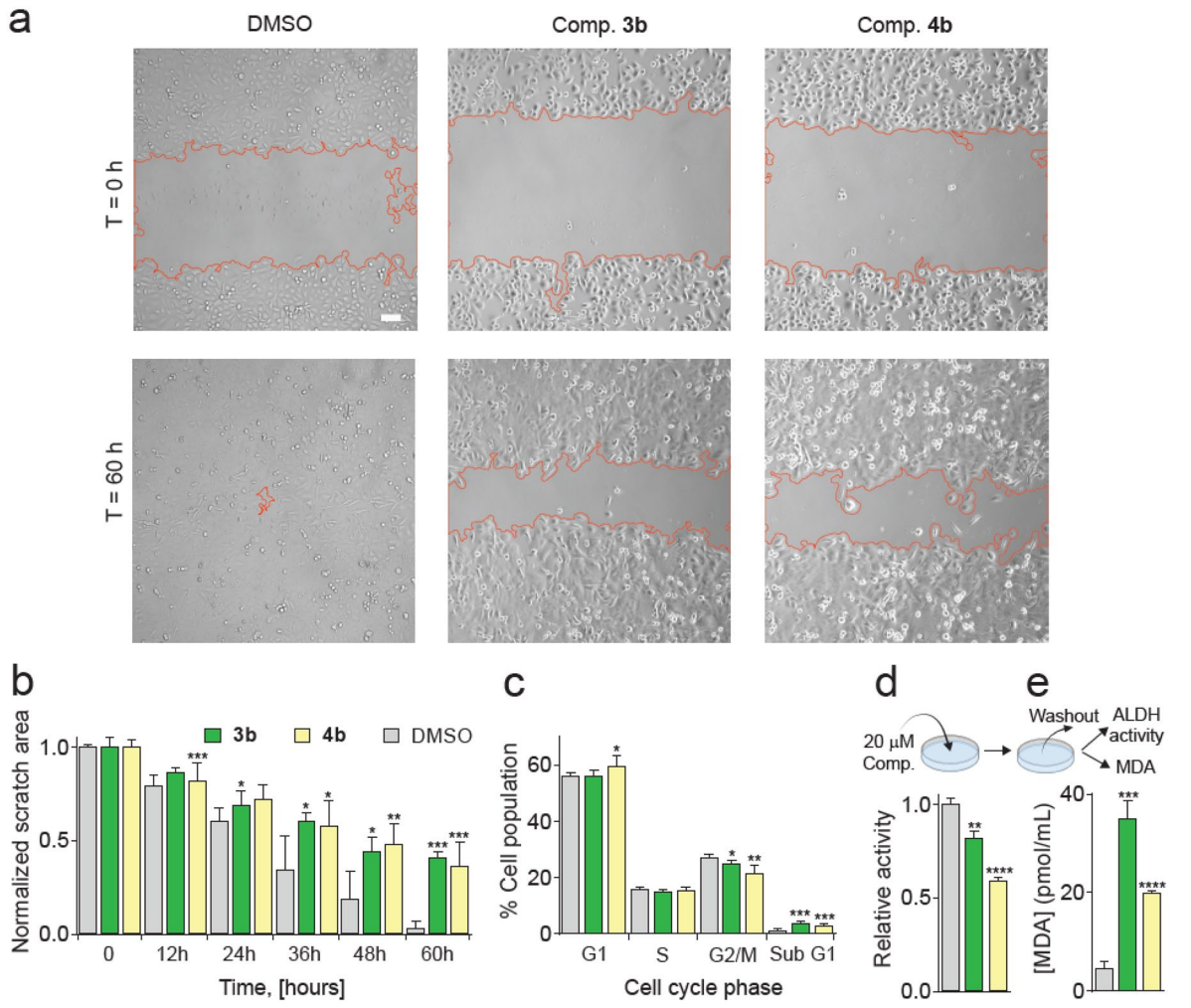

Figure 5. Effects of compound **3b** and **4b** in migration, cell cycle progression, and MDA accumulation in PCa cells. (a) Representative images of DU145 cells migration upon scratch generation in a confluent monolayer. Time point 0 h (T = 0 h) or 60 h (T = 60 h) points post-incubation in presence of DMSO, compound **3b** or compound **4b** at 20 µM final concentration, are shown. Scale bar = 100 µm. (b) Quantification of scratch area reduction over time normalised to the scratch area at T = 0 h. Wound healing was monitored at 12, 24, 36, 48 and 60 h post-incubation with the indicated compounds. (c) Quantification of cell cycle distribution in DU145 cells treated with DMSO, compound **3b** or compound **4b** at 20 µM final concentration for 24 h prior to cytofluorimetric analysis. The percentage of cells in each population is shown. (d) Total intracellular ALDH activity measured in DU145 cell lysates following pre-incubation with 20 µM **3b** or **4b** for 24 h at 37 °C. Cells were extensively washed prior to lysis to eliminate any non-covalently bound material. (e) Quantification of malondialdehyde (MDA) levels in the same cell lysates. MDA concentration was measured and normalised to the total protein content of each sample, as determined by the Bradford assay. In all plots, error bars represent the standard deviation, and asterisks indicate statistical significance levels: $p \leq 0.05$ (*), $p \leq 0.01$ (**), and $p \leq 0.001$ (***).

reported upon selective inhibition of ALDH1A3 with the reversible inhibitor NR6[51]. As for the more-than-proportional increase in MDA relative to ALDH inhibition, this can be explained by the chain-reaction nature of lipid peroxidation: even partial impairment of aldehyde detoxification may exceed cellular buffering capacity, leading to disproportionate MDA accumulation. Additionally, reactive aldehydes can further amplify oxidative stress. Consistently, ALDH7A1 has been shown to limit lipid peroxidation both by directly metabolising reactive aldehydes and by supporting FSP1-dependent antioxidant recycling, so even partial inhibition can significantly weaken this buffering system[52].

These results confirmed that our 1,2,4-oxadiazole derivatives counteract the protective role of ALDHs, thus eliciting cell toxicity through an increase in reactive oxygen species. Notably, a ~20–40% decrease in ALDH activity observed for **3b** or **4b** was enough to induce disproportionately large accumulations of MDA. This response could trigger a cascade effect in which even minor ALDH activity reductions disrupt the balance of reactive aldehyde clearance, leading to large increases in oxidative stress. Such

hypersensitivity to ALDH inhibition highlights the crucial role of ALDH7A1 in maintaining redox homeostasis and suggests its modulation could be leveraged for targeted oxidative stress therapies.

Conclusions

From an in-house library of BDHI derivatives, we identified a series of irreversible inhibitors of ALDH7A1 that covalently modify the catalytic cysteine residue, leading to sustained enzyme inhibition and reduced cellular viability and mobility in PCa cells. Inhibition produced accumulation of cells in the sub-G1 population, consistent with increased cell death, and produced a persistent reduction of intracellular ALDH activity and a pronounced accumulation of MDA, indicating a disruption of aldehyde detoxification pathways. Compounds **3b** and **4b** exhibited the highest potency and selectivity for ALDH7A1 over ALDH4A1, the first ALDH isoform reported to be inhibited by ACV derivatives, and GAPDH, a recognised target of BDHI derivatives. Covalent docking showed that the compounds can exploit a hydrophobic tunnel unique to ALDH7A1 to access the catalytic cysteine, promoting covalent engagement. In ALDH4A1, subtle polarity and steric differences hinder binding, explaining lower activity. These findings pave the way for the development of isoform-selective, irreversible ALDH inhibitors with potential applications in oncology.

Experimental

Chemical entities

The tested compounds were synthesised as previously reported[53–55]. Briefly, the 1,3,4-oxadiazoles **1a-4a** and the 1,2,4-oxadiazoles **1b-4b** were synthesised as depicted in Scheme S1 and Scheme S2, respectively, of the Supporting Information.

Synthesis of derivatives 1a-4a

Methyl 4-hydroxybenzoate (**5**) was treated with the desired alkyl bromide, in presence of K_2CO_3, to give intermediates **6–8**. Esters **6–8** were then converted into their respective hydrazides **11–13** by refluxing them in the presence of hydrazine hydrate in ethanol. The hydrazide **10** was synthesised starting from the corresponding acyl chloride **9**[56]. Reaction of **10–13** with acrylic acid using EDC·HCl in dry dichloromethane at room temperature afforded intermediates **14–17**. Afterwards, **14–17** were converted into the 1,3,4-oxadiazoles **18–21** using hexachloroethane, *N,N*-diisopropylethylamine and triphenylphosphine in acetonitrile at room temperature. Alkenes **18–21** reacted with bromonitrile oxide, generated *in situ* from its stable precursor dibromoformaldoxime (DBF) in the presence of solid $NaHCO_3$ and ethyl acetate, to give the final compounds **1a-4a**.

Synthesis of derivatives 1b-4b

4-Hydroxybenzaldehyde (**22**) was treated with the desired alkyl bromide, in presence of K_2CO_3, to give intermediates **23–26**. Nitriles **27–30** were synthesised in a one-pot procedure starting from aldehydes **23–26** by refluxing hydroxylamine hydrochloride and acetic anhydride in pyridine. Afterwards, the nitrile-substituted intermediates **27–30** were treated with hydroxylamine hydrochloride and Na_2CO_3 in a refluxing ethanol/water mixture to give amidoximes **31–34**. Intermediates **31–34** were converted into the corresponding *O*-acrylamidoximes **35–38** using acryloyl chloride in dry THF. **35–38** were converted into the 1,2,4-oxadiazoles **39–42** using a catalytic amount of TBAF in dry THF at room temperature. The final compounds **1b-4b** were synthesised as reported above for **1a-4a**, starting from alkenes **39–42**.

Protein expression, purification and characterisation

The expression vector encoding ALDH7A1 (EC:1.2.1.31, Uniprot P49419) was a gift from Nicola Burgess-Brown (Addgene plasmid # 38866). The expression vector encoding ALDH4A1 (EC:1.2.1.88,

Uniprot P30038) was a gift from Jack Tanner and Katrin Rittinger. The plasmids were transformed into *Escherichia coli* BL21 (DE3) cells (Thermo Fisher Scientific, Waltham, MA, USA). Protein expression was induced by adding 1 mM isopropyl-β-D-1-thiogalactopyranoside (IPTG) and incubating at 20 °C for 20 h. Cells were harvested by centrifugation, thoroughly washed, and resuspended in lysis buffer containing 50 mM Tris, 500 mM NaCl, 20 mM imidazole, 1.5 µM pepstatin A, 0.2 mM benzamidine, 0.2 mM PMSF, 1 mg/mL lysozyme, pH 8.0. Cell disruption was carried out by sonication. The proteins were purified via immobilised metal affinity chromatography (IMAC) using Talon Superflow™ resin (Cytiva, Marlborough, MA, USA), followed by dialysis against a buffer composed of 50 mM Tris, 50 mM NaCl, and 1 mM dithiothreitol (DTT), pH 7.8. The purified proteins were then concentrated, snap-frozen in liquid nitrogen, and stored at −80 °C in 50 µL aliquots at a final concentration of 70 µM. Protein purity was evaluated by 12% SDS-PAGE and densitometric analysis using a ChemiDoc imaging system (Bio-Rad, Hercules, CA, USA). Protein concentrations were determined by UV-visible absorbance at 280 nm using a Cary 4000 spectrophotometer (Agilent Technologies, Santa Clara, CA, USA), with an extinction coefficient of 82850 $M^{-1}cm^{-1}$ for ALDH7A1 and 80330 $M^{-1}cm^{-1}$ for ALDH4A1 (ProtParam, ExPASy). Prior to use, aliquots were thawed, centrifuged thoroughly, and protein concentration was reassessed spectrophotometrically. Human glyceraldehyde 3-phosphate dehydrogenase (GAPDH) encoded in a pET28 vector was expressed in *E. coli* BL21 (DE3) cells and purified by IMAC chromatography[35].

Size exclusion chromatography

The oligomerisation state of ALDH7A1 was analysed by SEC using an Agilent 1260 Infinity HPLC system (Agilent Technologies, Santa Clara, CA, USA) equipped with a Zenix-C SEC-150 column (Sepax Technologies, Newark, DE, USA). Detection was carried out at 280 nm. The column was equilibrated at 37 °C and developed in phosphate-buffered saline (PBS) at a constant flow rate of 0.35 ml/min. ALDH7A1 was injected at three different concentrations, i.e., 5 µM, 18 µM, and 83 µM. A calibration curve was generated using the following molecular weight standards: apoferritin (440 kDa), alcohol dehydrogenase (140 kDa), conalbumin (75 kDa), and myoglobin (17 kDa).

Enzyme assays

ALDH7A1 activity was measured using a direct assay based on the NAD^+-dependent oxidation of AcH to acetic acid. Reactions were carried out with 3 mM NAD^+ and 10 mM AcH, and the increase in absorbance at 340 nm, corresponding to NADH formation, was monitored using a Cary 4000 UV-Vis spectrophotometer (Agilent Technologies) or a HaloLED 96-well microplate reader (Control Tecnica, Padova, Italy). For kinetic analyses, the concentration of AcH was varied at a fixed NAD^+ concentration (2 mM), and enzyme concentration was set to 1 µM. Kinetic parameters were obtained by fitting the initial velocities (Vo) to the Michaelis–Menten equation. ALDH4A1 activity was assessed using Δ^1-pyrroline-5-carboxylate (P5C) as a substrate in a modified version of the ALDH7A1 assay. P5C was synthesised by periodate oxidation of hydroxylysine[57]. Briefly, 0.164 mmol hydroxylysine was dissolved in 2.33 ml water and cooled to 4 °C in the dark. A freshly prepared 3.67 ml solution of 50 mM sodium periodate was adjusted to pH 7.0 and added to the hydroxylysine solution. After 8 min on ice, excess periodate was quenched with 58.3 µL of 1 M glycerol. The mixture was incubated for 2 min on ice, acidified with 50 µL of 6 N HCl, and P5C concentration was quantified enzymatically using ALDH4A1, yielding a final concentration of 1.35 mM. Enzymatic reactions were conducted with 3 mM NAD^+ and 90 µM P5C. GAPDH activity was determined using 1.7 mM NAD^+ and 92 µM G3P as substrates in a buffered solution containing 10 mM triethanolamine (TEA), 10 mM Na_2HAsO_4, 5 mM EDTA, pH 7.6. The reaction was monitored by UV-vis absorption at 340 nm[35]. All enzyme assays were performed at 37 °C and in at least two independent replicates.

Molecular docking

Molecular docking calculations were carried out in Maestro v12.8 (Schrödinger release 2021–2; Schrödinger, LLC, New York, NY, 2025). The co-crystallized ligands and the BDHI covalent library, containing the **1-4a** and **1-4b** (*R*- and *S*-isomers), were prepared with LigPrep. For each ligand, a single

ionisation and tautomeric state was generated based on Epik predictions at pH = 7.0 ± 2.0. Crystal structures of ALDH7A1 and ALDH4A1 (PDB IDs 4ZUL and 3V9K, respectively) were imported into the Protein Preparation Wizard. The protonation state of ionisable residues was assigned at pH = 7.0 using pK_a values computed by PROPKA, the NAD^+ cofactor was modelled by molecular replacement based on structural alignment with PDB 4X0T. The resulting system underwent restrained minimisation with default settings (OPLS4 force field, heavy atoms were converged to RMSD = 0.30 Å). All crystallographic water molecules were removed prior to docking. Covalent docking studies were carried out with Maestro CovDock[58], with the reactive nucleophile being Cys302 in ALDH7A1 and Cys348 in ALDH4A1, and centreing the grid the co-crystallized ligands. In docking, residues of the binding site were kept rigid with the exception of Trp175, for which an alternative backbone-dependent rotamer (as observed in PDB 4X0T) was used to define an open conformation of the binding site. Aldehydes and semialdehydes were docked using the nucleophilic addition to a double bond protocol resulting in the corresponding tetrahedral intermediate, while the BDHI library was docked using the nucleophilic substitution protocol on SMARTS BrCI=NOCCl, with elimination of the halogen as the leaving group. A maximum of 20 poses was generated per ligand. Images were prepared using the PyMOL Molecular Graphics System (Version 3.0 Schrödinger, LLC).

Inhibition assays

Inhibitors were prepared as 50 mM stock solutions in DMSO. Enzymes were incubated at 2.5 µM final concentration with test compounds (20 µM final, unless otherwise stated) at 37 °C for 24 h in their respective buffer systems: 50 mM Tris, 50 mM NaCl, pH 7.8 for ALDH7A1 and ALDH4A1; and 10 mM TEA, 5 mM EDTA, 10 mM sodium arsenate, pH 7.6 for GAPDH. Prior stability assays indicated ~50% residual activity after 24 h in DMSO; therefore, non-treated controls were included throughout, and results were corrected for non-specific activity loss. After incubation, samples were centrifuged, and residual enzyme activity was measured using the protocols described above.

LC-MS/MS experiments

To assess which of the 10 cysteine residues in ALDH7A1 reacted with the test compounds, recombinant ALDH7A1 at a final concentration of 50 µM was incubated with 150 µM of **3b** for 24 h at 37 °C. The reaction was quenched with 1 mM cysteine, and the protein was precipitated overnight in 4 volumes of acetone at −20 °C. Pellets were resuspended in 50 mM Tris, 8 M urea, pH 8.0, supplemented with 5.5 mM TCEP and incubated at 30 °C for 2 h. Iodoacetamide was added at 10 mM final concentration and the mixture incubated at RT in the dark for 30 min. Samples were diluted with 50 mM Tris, pH 8.0 to reach a final concentration of 2 M urea and incubated overnight with trypsin 0.016 mg/ml at 30 °C. Digestion was stopped with 0.1% TFA. A control sample of ALDH7A1 incubated with DMSO in the absence of **3b** was processed identically. Peptides were analysed by LC-MS/MS using an Exploris 480 Orbitrap MS (Thermo Fisher Scientific, USA) coupled to an Ultimate 3000 Nano UHPLC. One µg of peptide per injection was loaded in triplicate onto a 75 µm × 500 mm Easy Nano C18 column (ES903, Thermo Fisher Scientific, USA). The Easy-Spray source was operated in positive mode (spray voltage 1.8 kV; ion transfer tube 275 °C; sheath gas 3; aux gas 8; sweep gas 0). Separation was performed at 45 °C with a 0.25 ml/min flow rate. Mobile phases: A = 0.1% FA in H_2O + 3% ACN; B = 0.1% FA in ACN + 3% H_2O. Gradient: 4–26% B (2–52 min), 26–50% (52–60 min), 50–95% (60–62 min), held at 95% (62–65.9 min), re-equilibrated at 4% B. Total run time: 120 min. Data were acquired in Full MS/dd-MS^2 (TOP20) mode over m/z 200–3000 (resolution: 120,000 for MS1; 15,000 for MS2). HCD fragmentation was performed (NCE = 28); dynamic exclusion: 55 s; charge states: 2–6. Instrument was calibrated prior to analysis. Raw files were processed in MaxQuant v2.6.7.0 with the Andromeda search engine against the ALDH7A1 sequence, decoy database, and common contaminants. Search parameters: min. peptide length = 7; 1% FDR at PSM, protein, and site level. Variable modifications were oxidation (M), N-term acetylation, cysteine carbamidomethylation, and a custom cysteine +285.11 Da modification for **3b** adducts. Modified peptides were filtered based on: PEP < 0.01, localisation probability > 0.75, localisation score > 40, delta score > 10, and precursor ion intensity > 1×10^8. The same workflow was applied to control samples. Fragment ion annotation and match scores were obtained using Skyline[59].

Cell culture

The PCa cells DU145 (#HTB-81, ATCC) and LNCaP (#CRL1740, ATCC) were cultured in an RPMI-1640 culture medium, supplemented with 10% foetal bovine serum (yourSIAL-FBS-SA, S.I.A.L. Group), 1% glutamine, and 1 mg/mL penicillin/streptomycin (Sigma Aldrich, Milan, Italy). Hs27 cells (#CRL1634, ATCC) were cultured in DMEM medium (Gibco™, Thermo Fisher Scientific, Waltham, MA, United States), supplemented with 10% foetal bovine serum, 1% glutamine, and 1 mg/mL penicillin/streptomycin. Cells were cultured in 10 cm dishes and maintained at 37 °C in an atmosphere of 5% CO_2. Hs27 cells were used between passage numbers 3 and 15.

Cell viability assay

Cells were seeded in a flat-bottom 96-well plate at 1×10^4 cells/well concentration, in complete medium. After 24 h, cells were treated with different concentrations (ranging from 1 µM to 100 µM) of ALDH inhibitors for 24 h, in serum-free medium. A DMSO control was used as a vehicle control at the highest concentration tested. At the end of the treatment, cell viability for adherent cells was measured by Crystal Violet assay[60]. Briefly, plates were washed with PBS, before incubation with 0.25% aqueous crystal violet staining solution for 20 min at RT. Cells were then washed with PBS and resuspended in a 20% Sodium Dodecyl Sulphate (SDS) solution. The absorbance (A595 nm) was measured by spectrophotometric analysis (MultiscanGo, ThermoFisher Scientific). At least three independent experiments were performed for each assay condition.

Cell cycle assay

Cell cycle phases (G1, S, G2/M) and the fraction of dead cells, identified by sub-G1 DNA content, were determined using propidium iodide (PI) staining followed by flow cytometric analysis, as previously reported[61,62]. Briefly, cells were fixed in 70% (v/v) cold ethanol and stained with PI (50 µg/mL) for 30 min at 4 °C in presence of RNase (250 µg/mL). Samples were analysed using a BD LSRFortessaTM X-20 cytofluorometer (BD Biosciences), and the resulting data were processed using FlowJo software (Tree Star, Inc.).

Wound healing assay

DU145 cells were seeded in 6-well plates and cultured in complete growth media until reaching confluency. A linear scratch was then introduced into the cell monolayer, and detached cells or debris were removed by washing with 1x PBS, before incubating with 20 µM of the indicated compounds. Cell migration was monitored using a Leica DMi8 inverted microscope (Leica THUNDER Imager Live Cell, Wetzlar, Germany) under controlled conditions (37 °C, humidified 5% CO_2 atmosphere). Phase-contrast images were acquired every 20 min for 60 h, using an x10 objective. Image analysis was performed using the Wound-Healing Size Tool plugin in the ImageJ software (version 2.1.0/1.53c) with the following settings: variance window radius 20, threshold value 20, percentage of saturated pixels 0.001, as previously described[8]. Statistical analyses and graphical representations were generated using R (version 4.2.1) and RStudio (version 2021.09.0)[63].

ALDH activity in cell lysates

To evaluate the residual ALDH activity in cells pre-treated with **3b** or **4b**, DU145 cells were grown in 10-cm dishes for 24 h. The cells were then incubated in RPMI containing **3b** or **4b** at 20 µM final concentration. After 24 h, the cells were collected, washed twice in PBS, and pelleted by centrifugation. The samples were flash-frozen and stored at −80 °C. The cell paste was thawed and resuspended in 150 µL of lysis buffer (PBS) and subjected to five freeze-thaw cycles. The resulting cell lysate was centrifuged at 16,000 × g for 40 min. Total protein concentration in the supernatant was determined by Bradford assay. ALDH activity was measured using the enzyme assay described above at 37 °C in a microplate by adding

either 20 µL of cell lysate or 20 µL of PBS as a control. Readings at 340 nm were collected over time with a HaloLED 96-well microplate reader (Control Tecnica, Padova, Italy). The initial velocities (Vo) were obtained by linear fitting of the timepoints and normalised to the protein content of each sample. All activity assays on cell lysates were performed at least in triplicate.

Malondialdehyde assays

The OxiSelect™ MDA Adduct Competitive ELISA Kit (Cell Biolabs Inc., San Diego, CA, USA) was used as per manufacturer's instructions. Briefly, samples corresponding to 11.5 µg of total proteins (Bradford assay) were added to each well. All the antibody incubations and the reaction with the Substrate Solution were performed at room temperature, and PBS was used as control. The colorimetric reaction was carried out for 10 s before the Stop Solution was added. A standard calibration curve was generated using MDA adduct concentrations of 1500, 750 and 375 pmol/mL, as described in the product manual. After the incubation, readings at 450 nm were collected with a HaloLED 96-well microplate reader. All MDA measurements on cell lysate were performed in at least three independent replicates.

Acknowledgements

The authors acknowledge the "Fondazione di Modena" for funding the UHPLC-Exploris 480 system at the Centro Interdipartimentale Grandi Strumenti (CIGS) of the University of Modena and Reggio Emilia, Italy. The authors thank the Interdepartmental Center of Services (CIS), Omics and Biobank, "Magna Græcia" University of Catanzaro, for providing access to facilities and instrumentations. This work has been carried out in the frame of the ALIFAR project, funded by the Italian Ministry of University through the program 'Dipartimenti di Eccellenza 2023–2027. The graphical abstract was created in BioRender. (Bruno, S. (2026) https://BioRender.com/arp1m41).

Author contributions

CRediT: **Raffaella Gallo**: Conceptualization, Formal analysis, Funding acquisition, Investigation, Writing – original draft; **Antonio Scarano**: Formal analysis, Investigation, Writing – original draft; **Eleonora Gianquinto**: Formal analysis, Funding acquisition, Investigation; **Gaia Franzini**: Formal analysis, Investigation; **Giulia Antonini**: Investigation; **Serena Montalbano**: Formal analysis, Investigation; **Camillo Palmieri**: Conceptualization, Funding acquisition, Supervision, Writing – original draft; **Paola Conti**: Funding acquisition, Supervision; **Francesca Spyrakis**: Conceptualization, Funding acquisition, Supervision, Writing – original draft; **Chiara Borsari**: Conceptualization, Funding acquisition, Supervision, Writing – original draft; **Stefano Bruno**: Conceptualization, Funding acquisition, Supervision, Writing – original draft.

Disclosure statement

No potential conflict of interest was reported by the author(s).

Funding

This work was supported by Guido Berlucchi Foundation Mini Grant (CANCERCOPE, grant number G43C23002440001) and by Umberto Veronesi Foundation (to C.B.). This study was supported by funds from University of Milan - Piano di sostegno alla Ricerca 2023- LINEA 2. We acknowledge the Programma di ricerca CN00000013 "National Centre for HPC, Big Data and Quantum Computing", finanziato dal Decreto Direttoriale di concessione del finanziamento n0.1031 del 17.06.2022 a valere sulle risorse del PNRR MUR - M4C2 - Investimento 1.4 - Avviso "Centri Nazionali" - D.D. n. 3138 del 16 dicembre 2021. R.G. is supported by Umberto Veronesi Foundation and Ferrero Foundation. We thank the University of Turin for funding support (SPYF_RILO_23_01; GIAE_RILO_24_02). We thank the University of Parma for financial support (BRUNO_S_FIL). This work was supported by Regione Calabria (Grant RF-2019–12370255 to C.P.).

Data availability statement

The datasets used and/or analysed during the current study are available from the corresponding author upon reasonable request.

References

1. Bray F, Laversanne M, Sung H, Ferlay J, Siegel RL, Soerjomataram I, Jemal A. Global cancer statistics 2022: GLOBOCAN estimates of incidence and mortality worldwide for 36 cancers in 185 countries. CA Cancer J Clin. 2024;74(3):229–263.
2. Kratzer TB, Mazzitelli N, Star J, Dahut WL, Jemal A, Siegel RL. Prostate cancer statistics, 2025. CA Cancer J Clin. 2025;75(6):485–497.
3. Achard V, Putora PM, Omlin A, Zilli T, Fischer S. Metastatic prostate cancer: treatment options. Oncology. 2022;100(1):48–59.
4. Obinata D, Takayama K, Inoue S, Takahashi S. Exploring androgen receptor signaling pathway in prostate cancer: a path to new discoveries. Int J Urol. 2024;31(6):590–597.
5. Coelho RS, Rocha SM, Maia CJ. Combined therapies with taxane-based chemotherapeutic drugs in prostate cancer: novel insights and future directions. Biochem (Basel). 2023;3(3):118–141.
6. Swami U, McFarland TR, Nussenzveig R, Agarwal N. Advanced prostate cancer: treatment advances and future directions. Trends Cancer. 2020;6(8):702–715.
7. Song Y, Hou Z, Zhu L, Chen Y, Li J. Oxidative stress as a catalyst in prostate cancer progression: unraveling molecular mechanisms and exploring therapeutic interventions. Discov Oncol. 2025;16(1):457.
8. Bossio S, Perri A, Gallo R, De Bartolo A, Rago V, La Russa D, Di Dio M, La Vignera S, Calogero AE, Vitale G, et al. Alpha-lipoic acid reduces cell growth, inhibits autophagy, and counteracts prostate cancer cell migration and invasion: evidence from in vitro studies. Int J Mol Sci. 2023;24(23):17111.
9. Rodríguez-Zavala JS, Calleja LF, Moreno-Sánchez R, Yoval-Sánchez B. Role of aldehyde dehydrogenases in physiopathological processes. Chem Res Toxicol. 2019;32(3):405–420.
10. Jiang Y, Song H, Jiang L, Qiao Y, Yang D, Wang D, Li J. Silybin prevents prostate cancer by inhibited the ALDH1A1 expression in the retinol metabolism pathway. Front Cell Dev Biol. 2020;8:574394.
11. Al Shareef Z, Kardooni H, Murillo-Garzón V, Domenici G, Stylianakis E, Steel JH, Rabano M, Gorroño-Etxebarria I, Zabalza I, Vivanco M. d, et al. Protective effect of stromal Dickkopf-3 in prostate cancer: opposing roles for TGFBI and ECM-1. Oncogene. 2018;37(39):5305–5324.
12. Zhang Z, Cheng L, Li J, Farah E, Atallah NM, Pascuzzi PE, Gupta S, Liu X. Inhibition of the Wnt/β-catenin pathway overcomes resistance to enzalutamide in castration-resistant prostate cancer. Cancer Res. 2018;78(12):3147–3162.
13. Gorodetska I, Offermann A, Püschel J, Lukiyanchuk V, Gaete D, Kurzyukova A, Freytag V, Haider M-T, Fjeldbo CS, Di Gaetano S, et al. ALDH1A1 drives prostate cancer metastases and radioresistance by interplay with AR- and RAR-dependent transcription. Theranostics. 2024;14(2):714–737.
14. Wang S, Zhou X, Liang C, Bao M, Tian Y, Zhu J, Zhang T, Yang J, Wang Z. ALDH1A3 serves as a predictor for castration resistance in prostate cancer patients. BMC Cancer. 2020;20(1):387.
15. Yan J, De Melo J, Cutz J-C, Aziz T, Tang D. Aldehyde dehydrogenase 3A1 associates with prostate tumorigenesis. Br J Cancer. 2014;110(10):2593–2603.
16. Püschel J, Dubrovska A, Gorodetska I. The multifaceted role of aldehyde dehydrogenases in prostate cancer stem cells. Cancers (Basel). 2021;13(18):4703.
17. Brocker C, Cantore M, Failli P, Vasiliou V. Aldehyde dehydrogenase 7A1 (ALDH7A1) attenuates reactive aldehyde and oxidative stress induced cytotoxicity. Chem Biol Interact. 2011;191(1-3):269–277.
18. Iglesias-Gato D, Wikström P, Tyanova S, Lavallee C, Thysell E, Carlsson J, Hägglöf C, Cox J, Andrén O, Stattin P, et al. The proteome of primary prostate cancer. Eur Urol. 2016;69(5):942–952.
19. Le Magnen C, Bubendorf L, Rentsch CA, Mengus C, Gsponer J, Zellweger T, Rieken M, Thalmann GN, Cecchini MG, Germann M, et al. Characterization and clinical relevance of ALDHbright populations in prostate cancer. Clin Cancer Res. 2013;19(19):5361–5371.
20. Lee J-S, Lee H, Woo SM, Jang H, Jeon Y, Kim HY, Song J, Lee WJ, Hong EK, Park S-J, et al. Overall survival of pancreatic ductal adenocarcinoma is doubled by Aldh7a1 deletion in the KPC mouse. Theranostics. 2021;11(7):3472–3488.
21. Van Den Hoogen C, Van Der Horst G, Cheung H, Buijs JT, Pelger RCM, Van Der Pluijm G. The aldehyde dehydrogenase enzyme 7A1 is functionally involved in prostate cancer bone metastasis. Clin Exp Metastasis. 2011;28(7):615–625.
22. Ketola K, Hilvo M, Hyötyläinen T, Vuoristo A, Ruskeepää A-L, Orešič M, Kallioniemi O, Iljin K. Salinomycin inhibits prostate cancer growth and migration via induction of oxidative stress. Br J Cancer. 2012;106(1):99–106.
23. Luo M, Gates KS, Henzl MT, Tanner JJ. Diethylaminobenzaldehyde is a covalent, irreversible inactivator of ALDH7A1. ACS Chem Biol. 2015;10(3):693–697.
24. Moreb JS, Ucar D, Han S, Amory JK, Goldstein AS, Ostmark B, Chang L-J. The enzymatic activity of human aldehyde dehydrogenases 1A2 and 2 (ALDH1A2 and ALDH2) is detected by Aldefluor, inhibited by diethylaminobenzaldehyde and has significant effects on cell proliferation and drug resistance. Chem Biol Interact. 2012;195(1):52–60.
25. Muramoto GG, Russell JL, Safi R, Salter AB, Himburg HA, Daher P, Meadows SK, Doan P, Storms RW, Chao NJ, et al. Inhibition of aldehyde dehydrogenase expands hematopoietic stem cells with radioprotective capacity. Stem Cells Dayt. Ohio. 2010;28(3):523–534.

26. Ma M, He W, Zhao K, Xue L, Xia S, Zhang B. Targeting aldehyde dehydrogenase for prostate cancer therapies. Front Oncol. 2022;12:1006340.
27. Chen Y, Li X. Aldehyde Dehydrogenases as Promising Targets for Treating Toxic Alde-hyde-related Diseases. Curr Med Chem. 2024;31(8):970–994.
28. Hidalgo M, Rodriguez G, Kuhn JG, Brown T, Weiss G, MacGovren JP, Von Hoff DD, Rowinsky EK. A Phase I and pharmacological study of the glutamine antagonist acivicin with the amino acid solution aminosyn in patients with advanced solid malignancies. Clin Cancer Res Off J Am Assoc Cancer Res. 1998;4:2763–2770.
29. Chittur SV, Klem TJ, Shafer CM, Davisson VJ. Mechanism for acivicin inactivation of triad glutamine amidotransferases. Biochemistry. 2001;40(4):876–887.
30. Oliveira de Souza J, Dawson A, Hunter WN. An improved model of the Trypanosoma brucei CTP synthetase glutaminase domain-acivicin complex. ChemMedChem. 2017;12(8):577–579.
31. Allen L, Meck R, Yunis A. The inhibition of gamma-glutamyl transpeptidase from human pancreatic carcinoma cells by (alpha S,5S)-alpha-amino-3-chloro-4,5-dihydro-5-isoxazoleacetic acid (AT-125; NSC-163501). Res Commun Chem Pathol Pharmacol. 1980;27(1):175–182.
32. Smith TK, Ikeda Y, Fujii J, Taniguchi N, Meister A. Different sites of acivicin binding and inactivation of gamma-glutamyl transpeptidases. Proc Natl Acad Sci U S A. 1995;92(6):2360–2364.
33. Pinto A, Tamborini L, Cullia G, Conti P, De Micheli C. Inspired by nature: the 3-Halo-4,5-dihydroisoxazole moiety as a novel molecular warhead for the design of covalent inhibitors. ChemMedChem. 2016;11(1):10–14.
34. Kreuzer J, Bach NC, Forler D, Sieber SA. Target discovery of acivicin in cancer cells elucidates its mechanism of growth inhibition†Electronic supplementary information (ESI) available: synthesis, cloning, protein expression, purification and biochemical assays. See DOI:. Chem Sci. 2014;6(1):237–245.
35. Bruno S, Margiotta M, Pinto A, Cullia G, Conti P, De Micheli C, Mozzarelli A. Selectivity of 3-bromo-isoxazoline inhibitors between human and Plasmodium falciparum glyceraldehyde-3-phosphate dehydrogenases. Bioorg Med Chem. 2016;24(12):2654–2659.
36. Galbiati A, Zana A, Conti P. Covalent inhibitors of GAPDH: from unspecific warheads to selective compounds. Eur J Med Chem. 2020;207:112740.
37. Galbiati A, Bova S, Pacchiana R, Borsari C, Persico M, Zana A, Bruno S, Donadelli M, Fattorusso C, Conti P. Discovery of a spirocyclic 3-bromo-4,5-dihydroisoxazole covalent inhibitor of hGAPDH with antiproliferative activity against pancreatic cancer cells. Eur J Med Chem. 2023;254:115286.
38. Galbiati A, Zana A, Borsari C, Persico M, Bova S, Tkachuk O, Corfu AI, Tamborini L, Basilico N, Fattorusso C, et al. Role of stereochemistry on the biological activity of nature-inspired 3-Br-acivicin isomers and derivatives. Molecules. 2023;28(7):3172.
39. Pacchiana R, Mullappilly N, Pinto A, Bova S, Forciniti S, Cullia G, Dalla Pozza E, Bottani E, Decimo I, Dando I, et al. 3-Bromo-isoxazoline derivatives inhibit GAPDH enzyme in PDAC cells triggering autophagy and apoptotic cell death. Cancers (Basel). 2022;14(13):3153.
40. Korasick DA, Tanner JJ, Henzl MT. Impact of disease-linked mutations targeting the oligomerization interfaces of aldehyde dehydrogenase 7A1. Chem Biol Interact. 2017;276:31–39.
41. Luo M, Tanner JJ. Structural basis of substrate recognition by aldehyde dehydrogenase 7A1. Biochemistry. 2015;54(35):5513–5522.
42. Brocker C, Lassen N, Estey T, Pappa A, Cantore M, Orlova VV, Chavakis T, Kavanagh KL, Oppermann U, Vasiliou V. Aldehyde dehydrogenase 7A1 (ALDH7A1) is a novel enzyme involved in cellular defense against hyperosmotic stress. J Biol Chem. 2010;285(24):18452–18463.
43. Boström J, Hogner A, Llinàs A, Wellner E, Plowright AT. Oxadiazoles in medicinal chemistry. J Med Chem. 2012;55(5):1817–1830.
44. Srivastava D, Singh RK, Moxley MA, Henzl MT, Becker DF, Tanner JJ. The three-dimensional structural basis of type II hyperprolinemia. J Mol Biol. 2012;420(3):176–189.
45. Riveros-Rosas H, González-Segura L, Julián-Sánchez A, Díaz-Sánchez ÁG, Muñoz-Clares RA. Structural determinants of substrate specificity in aldehyde dehydrogenases. Chem Biol Interact. 2013;202(1-3):51–61.
46. Bogner AN, Stiers KM, McKay CM, Becker DF, Tanner JJ. Structural basis for the stereospecific inhibition of the dual proline/hydroxyproline catabolic enzyme ALDH4A1 by trans-4-hydroxy-L-proline. Protein Sci. 2021;30(8):1714–1722.
47. Jones KH, Lindahl R, Baker DC, Timkovich R. Hydride transfer stereospecificity of rat liver aldehyde dehydrogenases. J Biol Chem. 1987;262(23):10911–10913.
48. Dozmorov MG, Hurst RE, Culkin DJ, Kropp BP, Frank MB, Osban J, Penning TM, Lin H-K. Unique patterns of molecular profiling between human prostate cancer LNCaP and PC-3 cells. Prostate. 2009;69(10):1077–1090.
49. Mondal D, Narwani D, Notta S, Ghaffar D, Mardhekar N, Quadri SSA. Oxidative stress and redox signaling in CRPC progression: therapeutic potential of clinically-tested Nrf2-activators. Cancer Drug Resist. 2021;4(1):96–124.
50. Marnett LJ. Lipid peroxidation-DNA damage by malondialdehyde. Mutat Res. 1999;424(1-2):83–95.
51. Boumya S, Fallarini S, Siragusa S, Petrarolo G, Aprile S, Audrito V, La Motta C, Garavaglia S, Moro L, Pinton G. A selective ALDH1A3 inhibitor impairs mesothelioma 3-D multicellular spheroid growth and neutrophil recruitment. Int J Mol Sci. 2023;24(7):6689.

52. Yang J-S, Morris AJ, Kamizaki K, Chen J, Stark J, Oldham WM, Nakamura T, Mishima E, Loscalzo J, Minami Y, et al. ALDH7A1 protects against ferroptosis by generating membrane NADH and regulating FSP1. Cell. 2025;188(10):2569–2585.e20.
53. Borsari C, Santarem N, Coertzen D, Mazzolari A, Corfu AI, Coelho C, Barbosa F, Tamborini L, Birkholtz L-M, Raffellini L, et al. From pan-active to parasite-selective antiparasitic agents: a scaffold hopping approach. Eur J Med Chem. 2025;300:118095.
54. Corfu AI, Santarem N, Luelmo S, Mazza G, Greco A, Altomare A, Ferrario G, Nasta G, Keminer O, Aldini G, et al. Discovery of 1,3,4-oxadiazole derivatives as broad-spectrum antiparasitic agents. ACS Infect Dis. 2024;10(6):2222–2238.
55. Galbiati A, Zana A, Coser C, Tamborini L, Basilico N, Parapini S, Taramelli D, Conti P. Development of potent 3-Br-isoxazoline-based antimalarial and antileishmanial compounds. ACS Med Chem Lett. 2021;12(11):1726–1732.
56. Dumur F, Contal E, Wantz G, Phan TNT, Bertin D, Gigmes D. Immobilization of styrene-substituted 1,3,4-oxadiazoles into thermoreversible luminescent organogels and their unexpected photocatalyzed rearrangement. Chemistry. 2013;19(4):1373–1384.
57. Wu GY, Seifter S. Periodate oxidation products of hydroxylysine in the synthesis of 5-substituted prolines. Anal Biochem. 1985;147(1):103–107.
58. Zhu K, Borrelli KW, Greenwood JR, Day T, Abel R, Farid RS, Harder E. Docking covalent inhibitors: a parameter free approach to pose prediction and scoring. J Chem Inf Model. 2014;54(7):1932–1940.
59. MacLean B, Tomazela DM, Shulman N, Chambers M, Finney GL, Frewen B, Kern R, Tabb DL, Liebler DC, MacCoss MJ. Skyline: an open source document editor for creating and analyzing targeted proteomics experiments. Bioinformatics. 2010;26(7):966–968.
60. Ravi A, Palamiuc L, Loughran RM, Triscott J, Arora GK, Kumar A, Tieu V, Pauli C, Reist M, Lew RJ, et al. PI5P4Ks drive metabolic homeostasis through peroxisome-mitochondria interplay. Dev Cell. 2021;56(11):1661–1676.e10.
61. Ashford AL, Dunkley TPJ, Cockerill M, Rowlinson RA, Baak LM, Gallo R, Balmanno K, Goodwin LM, Ward RA, Lochhead PA, et al. Identification of DYRK1B as a substrate of ERK1/2 and characterisation of the kinase activity of DYRK1B mutants from cancer and metabolic syndrome. Cell Mol Life Sci. 2016;73(4):883–900.
62. Vecchio E, Gallo R, Mimmi S, Gentile D, Giordano C, Straface E, Marino R, Caiazza C, Pastore A, Ruocco MR, et al. FABP5 is a key player in metabolic modulation and NF-κB dependent inflammation driving pleural mesothelioma. Commun Biol. 2025;8(1):324.
63. Gallo R, Rai AK, McIntyre ABR, Meyer K, Pelkmans L. DYRK3 enables secretory trafficking by maintaining the liquid-like state of ER exit sites. Dev Cell. 2023;58(19):1880–1897.e11.